

MgII LINE VARIABILITY OF HIGH LUMINOSITY QUASARS

JONG-HAK WOO

Department of Physics, University of California Santa Barbara, CA 93106-9530 and
Yale Center for Astronomy and Astrophysics, Yale University, New Haven, CT 06520-8101

(Received 2007 October 9; Accepted 2008 March 2)

ABSTRACT

We monitored five high-luminosity quasars with $\lambda L_{3000\text{\AA}} > 10^{45} \text{ erg s}^{-1}$ at $0.4 \lesssim z \lesssim 0.6$ to measure flux variability of the MgII $\lambda 2798$ line and explore feasibility of reverberation mapping using MgII. Over the two year monitoring program, imaging data were obtained with the A Noble Double-Imaging Camera on the 1.3-m telescope at the Cerro Tololo Inter-American Observatory (CTIO), while spectroscopic data were obtained at the same night with the R-C spectrograph on the 1.5-m telescope at the CTIO. By performing differential photometry using available field stars in each quasar image, we measured variability – 10%-24% peak-to-peak changes and 3%-8% rms variations – in the B band, which includes flux changes in the rest-frame UV continuum ($\sim 2500\text{\AA}$ – $\sim 3600\text{\AA}$) as well as the MgII line. Utilizing photometric measurements for spectroscopic flux calibration, we measured the MgII line flux and the continuum flux at 3000\AA from each single-epoch spectrum. Four objects showed MgII line flux variability with 23%-50% peak-to-peak changes and 8%-17% rms variations over 1-1.5 year rest-frame time scales, while one object showed no MgII flux variability within the measurement error ($< 5\%$). We also detected 4%-15% rms variations of the MgII line width for all five objects. With synchronous observations for photometry and spectroscopy, we demonstrated the feasibility of the MgII line reverberation mapping for high-luminosity quasars at intermediate redshift.

Subject headings: galaxies: active — galaxies: nuclei — quasars: general

1. INTRODUCTION

Determining black hole mass is a fundamental step to understand the physics of the AGN accretion disk (e.g. Bonning et al. 2007; Davis et al. 2007) as well as cosmic evolution of black holes and galaxies (e.g. Di Matteo et al. 2005; Croton et al. 2006; Woo et al. 2006; Treu et al. 2007). Active galaxies with broad emission lines provide a way of estimating black hole masses, assuming that the motion of the broad-line regions (BLR) is dominated by the gravitational potential of the central source. Thus, virial mass can be determined from the dynamics of the BLR. The width of broad-emission lines are used in estimating the velocity scale, while the size (R_{BLR}) can be determined by measuring the time lag between the continuum flux changes (presumably originating from an accretion flow) and the corresponding flux changes in the broad-emission lines (Blanford & McKee 1982).

So far, reverberation masses have been determined for about three dozens of local Seyfert galaxies and PG quasars, which are limited to redshift $z < 0.4$ and optical luminosity $L_{5100\text{\AA}} < 10^{46} \text{ erg s}^{-1}$ (Wandel et al. 1999; Kaspi et al. 2000, Peterson et al. 2004), while there are numerous AGNs with higher optical luminosity at $z > 0.4$. Thus, it is crucial to increase the sample size, especially including higher luminosity and higher redshift AGNs, in order to validate the virial technique and understand its uncertainties. The size-luminosity relation – correlation between the measured time lag (BLR size) and the continuum luminosity (Kaspi et al. 2005; Bentz et al. 2006) – provides a simple recipe for black hole mass estimation without reverberation mapping (e.g. Woo & Urry 2002; Vestergaard 2002; Netzer & Trakhtenbrot

2007; McGill et al. 2007). Therefore, measuring time lags for higher luminosity AGNs is also necessary to validate the size-luminosity relation and avoid extrapolations in estimating black hole masses for high luminosity and high redshift quasars (e.g. McLure & Dunlop 2004; Vestergaard 2004).

Depending on the redshift of the source, different broad emission lines can be used for reverberation studies. For local AGNs, the best studied Balmer lines, such as H β and H α , showed clear correspondence to the continuum changes (e.g. Peterson et al. 2004). At $z > 2$, CIV $\lambda 1549$ and Ly α lines are redshifted in the optical range and become useful for reverberation studies with optical spectrographs. Recently, Kaspi et al. (2007) showed feasibility of reverberation mapping for quasars at $z > 2$, reporting CIV line flux variability for six quasars and a tentative time lag measurement for one object. In the same study, however, the Ly α line showed no flux variability within 5% measurement error. In the local universe, time lag measurements with CIV line have been reported for several Seyfert galaxies (see Peterson et al. 2004, for a summary).

At intermediate redshift, $0.7 < z < 2$, the MgII $\lambda 2798$ line becomes virtually the only available broad line for estimating virial black hole masses. However, there has been only a handful of studies on MgII line flux variability, and it is not clear whether the MgII line shows the same reverberation as other broad lines. For example, Clavel et al. (1991) reported that MgII line flux variability of NGC 5548 was much lower than flux changes in other broad lines and did not show clear correspondence to UV continuum flux changes. In the case of NGC 3516, the MgII line flux was almost constant in 1996 although other lines and the continuum showed large flux variations (Goad et al. 1999). In contrast, time-lag measure-

ments were consistent between MgII and Balmer lines for NGC 3783 (Reichert et al. 1994) and NGC 4151 (Metzroth et al. 2006). At high redshift, $1 < z < 2$, Trevese et al. (2007) studied two high-luminosity quasars and detected MgII line flux variability for one object. Clearly, flux variability of the MgII line has to be better constrained to test feasibility of reverberation mapping, especially for intermediate-to-high redshift quasars.

We initiated a monitoring program to study MgII line variability and explore feasibility of reverberation mapping for bright quasars with the 1.5-m and 1.3-m telescopes at the Cerro Tololo Inter-American Observatory (CTIO) when these telescopes became available in service mode through the Small and Moderate Aperture Research Telescope System (SMARTS) consortium¹ in 2003. In this paper we report our imaging and spectroscopic study on the MgII line variability of five high-luminosity quasars at $0.4 < z < 0.6$. The goal of the paper is to investigate variability of the MgII line flux and width. The paper is organized as follows. In § 2 we describe observations and data reduction. In § 3 we describe our measurements of B band luminosity variability and MgII line flux variability. In § 4 we discuss our results and their implications. A standard cosmology is assumed where necessary ($H_0 = 70 \text{ km s}^{-1} \text{ Mpc}^{-1}$, $\Omega_m = 0.3$ and $\Omega_\Lambda = 0.7$).

2. OBSERVATIONS AND DATA REDUCTION

2.1. Sample Selection and Experimental Design

To study feasibility of reverberation mapping with the MgII line, a sample of bright southern quasars was selected from the Calan-Tololo Survey catalogue (Maza et al. 1993, 1995, 1996) with a redshift range, $0.4 \lesssim z \lesssim 1$, where no reverberation study has been reported. Twelve bright objects were initially selected based on the observability of more than 6 months per year. Here we present five best observed objects with high quality spectra and strong MgII lines, observed at more than 5 different epochs for spectroscopy and photometry. Target properties of these objects are listed in Table 1. The other seven objects were excluded in this study due to the fact that observed spectra have lower signal-to-noise ratio ($\lesssim 10$), not enough to measure line flux variations with $\sim 5\%$ measurement errors, and/or the number of observed epochs with both photometry and spectroscopy is typically less than 5.

We designed spectroscopic and photometric observations to be carried out at the same night so that spectroscopic flux calibration can be accurately obtained using photometric measurements, assuming that there is no intra-night flux variations (see §3.2). However, because of the difficulty of scheduling, there are several epochs when spectroscopy and photometry were carried out at different nights. We excluded data from those epochs for the analysis of the MgII line flux variations (see Table 2).

2.2. Photometry

Photometric and spectroscopic observations were performed in service mode, respectively, with the CTIO 1.3-m and 1.5-m telescopes operated by the SMARTS consortium between March 2003 and February 2005. Due to

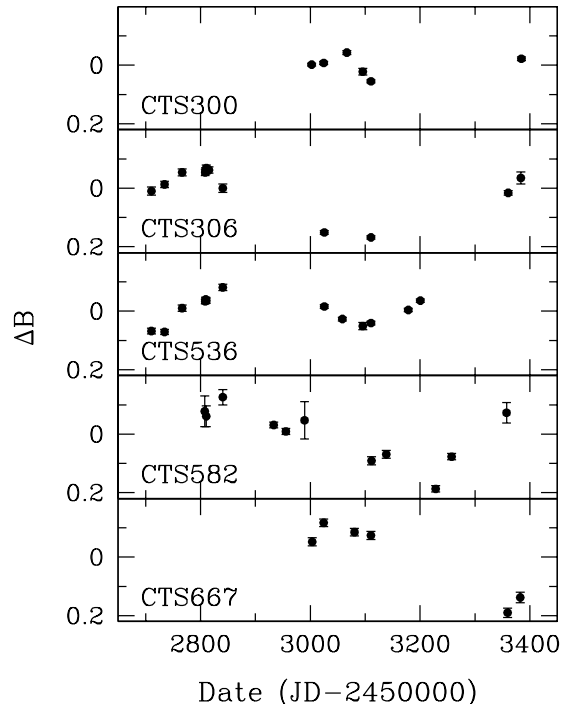


FIG. 1.— B band (rest-frame $\sim 2500\text{\AA}$ – $\sim 3600\text{\AA}$) light curves of all five objects. Peak-to-peak variations are 9%–24% and rms variations are 3%–8%, calculated in logarithmic scale.

the observability and limited telescope time, ~ 10 single-epoch data were obtained for given objects during the monitoring program. Table 2 shows journal of observations.

For photometry, we used the A Noble Double-Imaging Camera (ANDICAM), a dual-channel optical IR imager at the CTIO 1.3-m telescope. The optical CCD with an excellent cosmetics provided $\sim 6 \times 6$ arcminute² field of view and $0.369''$ per pixel resolution. Each target quasar was roughly centered in the field of view to cover as many as possible field stars for differential photometry. We used the broad B band filter to match the observed wavelength range in spectroscopy, in order to do spectroscopic flux calibration using photometric measurements. The typical exposure time was 10 minute, yielding signal-to-noise ratio (S/N) > 100 on the target quasars. Bias and dome flats were taken in the afternoon before each night. A set of standard stars were also taken during the night. Initial data reduction, including bias subtraction and flat-fielding, has been automatically performed through a pipeline by the Yale SMARTS team.

2.3. Spectroscopy

We used the R-C spectrograph with the 600 line mm^{-1} grating centered at $\sim 4500\text{\AA}$. The observed spectral range was ~ 3500 – 5300\AA , covering the MgII line (rest wavelength $\sim 2798\text{\AA}$) near the center in the observed spectral range. The pixel scale corresponded to 1.47\AA and the spatial scale along the slit was $1''.3$ per pixel. We chose the $2''$ wide slit to include most of the AGN light within the slit under the typical sub-arcsecond seeing conditions at the CTIO. The spectral resolution measured from arc lines was $\sim 3.8\text{\AA}$ (FWHM), yielding Gaussian velocity of 110 km s^{-1} at the center of the spectral

¹ <http://www.astro.yale.edu/smarts>

TABLE 1
TARGET PROPERTIES

(1) Name	(2) z	(3) RA (J2000)	(4) DEC (J2000)	(5) B	(6) log M_{BH}	(7) L/L_{Edd}
CTS300	0.352	11 28 18.62	-13 19 28.7	17.2	8.74	0.12
CTS306	0.456	11 59 41.02	-19 59 24.7	17.2	8.87	0.13
CTS536	0.500	14 01 49.27	-24 55 30.3	16.5	8.81	0.40
CTS582	0.483	22 40 18.84	-52 31 52.4	17.8	8.75	0.13
CTS667	0.557	11 39 10.70	-13 50 43.6	16.7	8.62	1.12

NOTE. — Col. (1): Target ID. Col. (2): Redshift measured from the MgII line. Col. (3): RA. Col. (4): DEC. Col. (5): mean B magnitude. Col. (6): black hole mass estimated using the MgII FWHM and the continuum luminosity at 3000\AA from the mean spectra. Col. (7): Eddington ratio calculated using black hole mass and $5.9 \times L_{3000\text{\AA}}$ as bolometric luminosity.

TABLE 2
JOURNAL OF OBSERVATIONS

Date (1)	Photometry Targets (2)	Spectroscopy Targets (3)
2003 Mar 12	CTS306, CTS536	CTS306, CTS536
2003 Apr 4		CTS306 ^a , CTS536 ^a
2003 Apr 5	CTS306, CTS536	
2003 May 7	CTS306, CTS536	CTS306, CTS536
2003 Jun 17	CTS582	CTS536 ^a , CTS582
2003 Jun 18	CTS306, CTS536	
2003 Jun 19	CTS306, CTS536	
2003 Jun 20	CTS306, CTS536, CTS582	
2003 Jun 25	CTS306	CTS306
2003 Jul 20	CTS306, CTS536, CTS582	CTS306, CTS536
2003 Sep 23		CTS582 ^a
2003 Oct 21	CTS582	CTS582
2003 Nov 12	CTS582	CTS582
2003 Dec 16	CTS582	CTS582
2003 Dec 19	CTS300	
2003 Dec 20	CTS667	
2003 Dec 29		CTS300 ^b
2003 Dec 30		CTS667 ^b
2004 Jan 20	CTS300, CTS667	CTS667
2004 Jan 21	CTS306, CTS536	CTS306, CTS536
2004 Feb 23	CTS536	CTS536
2004 Mar 2	CTS300	CTS300
2004 Mar 16	CTS667	CTS667
2004 Mar 31	CTS300, CTS536	CTS300, CTS536
2004 Apr 15	CTS300, CTS306, CTS536, CTS667	CTS300, CTS306, CTS536, CTS667
2004 Apr 16	CTS582	CTS582
2004 May 13	CTS582	
2004 Jun 22	CTS536	CTS536, CTS582 ^b
2004 Jul 14	CTS536	CTS536
2004 Aug 11	CTS582	
2004 Sep 9	CTS582	
2004 Nov 16		CTS582 ^b
2004 Dec 18	CTS582	CTS582
2004 Dec 20	CTS667	CTS667
2004 Dec 21	CTS306	CTS306
2004 Dec 22		CTS300 ^b
2005 Jan 12	CTS667	CTS667
2005 Jan 13	CTS306	
2005 Jan 14	CTS300	CTS300
2005 Jan 15		CTS306 ^b
2005 Feb 8		CTS300 ^b
2005 Feb 9		CTS667 ^b

REFERENCES. — a) these spectra were flux calibrated with photometric measurements from the previous or following night. b) these spectra were excluded in the analysis of MgII line flux variability due to the lack of photometric data

NOTE. — Col. (1): Observing date. Col. (2): Photometry targets Col. (3): Spectroscopy targets

range. Total exposure time for each object was 3600 second, divided into 3 exposures in order to remove cosmic rays, yielding $S/N \sim 10$ -30 per pixel on the continuum. Internal lamp flats were taken in the afternoon to correct pixel-to-pixel variations. A set of spectrophotometric standards were observed during each night for initial flux calibrations (see §3.2).

We performed the standard data reduction including bias subtraction, flat fielding, wavelength calibration, spectral extraction, and flux calibration using a series of IRAF scripts. He and Ar arc lines were used for wavelength calibration. One-dimensional spectra were extracted for maximal S/N with a typical extraction radius of 3 pixels, corresponding to $\sim 3.9''$. Individual spectra were combined with inverse-variance weighting to create the final spectrum for each single-epoch. For each night, we obtained sensitivity function using spectrophotometric stars. The flux scale is consistent within 1% rms variation over the monitoring period.

3. MEASUREMENTS

In this section, we present broad-band flux variability measured from differential photometry (§3.1). Then we show our spectroscopic analysis for MgII line variability. First, we demonstrate spectroscopic flux calibration with photometric measurements (§3.2). In §3.3 we present how we subtract the continuum and measure the MgII line flux. We report MgII line flux variability in §3.4, and MgII line width variability in §3.5.

3.1. B band flux variability from photometry

To measure the broad band flux variability, we performed differential photometry using stars in the field of each quasar, as demonstrated in the paper by Woo et al. (2007). More than 10 stars were initially used to check variability and photometric errors. Aperture photometry of comparison stars and quasars was performed using the PHOT task in IRAF, with a 10 pixel (corresponding to $13''$) aperture and with an annulus between 15 and 20 pixels for sky subtraction, based on our initial tests with images of various quality seeing. Photometric errors of individual stars were typically less than 1%. We chose three to five unsaturated stars brighter than each quasar for differential photometry. First, we calculated the magnitude difference between each comparison star and the target quasar. Second, we normalized the magnitude difference to zero by subtracting the mean difference over all observed epochs. Photometric errors of comparison stars were added in quadrature and then the photometric error of the target quasar was added on top of it, yielding total errors of $\sim 1\%$ for relative flux changes.

In Figure 1 we show relative B band flux variability. All five quasars showed significant flux variability in the B band. We find peak-to-peak variations in the range of 9%-24% and rms variations² in the range of 3%-8%. We note that since the MgII line flux is also included in the B band photometry, B band flux variability cannot be considered as the continuum (such as 3000Å) variability unless the MgII line flux is constant (see §3.4 for more details). Nevertheless, the detected B band flux varia-

tions clearly demonstrate that our sample quasars have UV continuum variability.

3.2. flux calibration using photometric measurements

The flux uncertainty of the ground-based spectroscopy is typically larger than 10% due to the slit losses, sky transparency, and various seeing conditions. In reverberation mapping studies, non-varying narrow emission lines, such as [O III] originated from far extended low-density regions, are used as an internal flux calibrator. Thus, flux variations of broad lines can be measured by normalizing each spectrum to a constant flux of the narrow line (e.g. Peterson et al. 1998; Woo et al. 2007). In the vicinity of the MgII line, there is no strong narrow line useful as an internal flux calibrator. The [OII] line at 3727Å is far from MgII in spectral range and much weaker than MgII, not desirable as an internal calibrator. However, since the MgII line is much stronger than $H\beta$, measuring its relative variation can be robustly done even without an internal flux calibrator as we demonstrate below.

Instead of relying on the precision of flux calibration with spectrophotometric stars, we normalize each single-epoch spectrum to match photometric measurements obtained at the same night. Using B band response function, we calculate synthetic magnitude from the observed spectrum and then normalize the spectrum by multiplying a scale factor in order to match the B band magnitude measured from photometry. The amount of flux calibration with a scale factor was typically 10%-20% of the original flux.

We note that spectroscopy and photometry observations were not performed at the exact same time. Thus, spectroscopic flux calibration is uncertain within the level of intra-night variations, which seem to be negligible for Seyfert 1 galaxies and quasars based on the study by Webb & Malkan (2000). Due to the limited telescope time for photometry, we have not attempted to measure intra-night variations for individual objects, which can be tested in the future.

3.3. MgII line and continuum flux measurements

Using the flux calibrated spectra, we measure the flux and width of the MgII line in several steps as similarly done in other studies (e.g. McGill et al. 2007). First, we fit the continuum under MgII with a straight line using the average flux around $\sim 2700\text{\AA}$ and $\sim 2900\text{\AA}$ with 40Å wide windows. We linearly interpolate these two continuum points to define an underlying continuum. Second, we measure the MgII line flux by integrating the flux using the continuum subtracted spectrum. We note that defining a true continuum under the MgII line is not straight forward because of the presence of broad FeII emission blends (small blue bump). Hence, depending on how the underlying continuum is defined, the measured MgII line flux can vary. Nevertheless, as far as we keep the same windows for determining the continuum, we can measure the relative changes in the MgII line flux between two different epochs. We did not subtract the broad FeII emission, which could contribute small amount of flux to the wings of the MgII line. However, the relative flux changes in MgII will not be significantly affected by the contribution of the FeII emission.

² We calculate rms variations using fluxes in logarithmic scale throughout the paper.

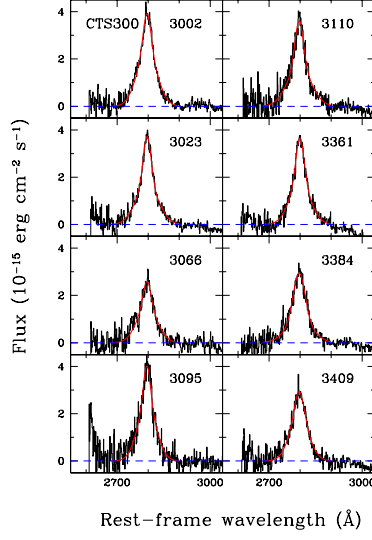


FIG. 2.— A series of continuum subtracted spectra around the MgII line of CTS300. The MgII lines are modeled with a multi-Gaussian profile (red). Observing dates (JD-2450000) are denoted in the upper right corner of each panel.

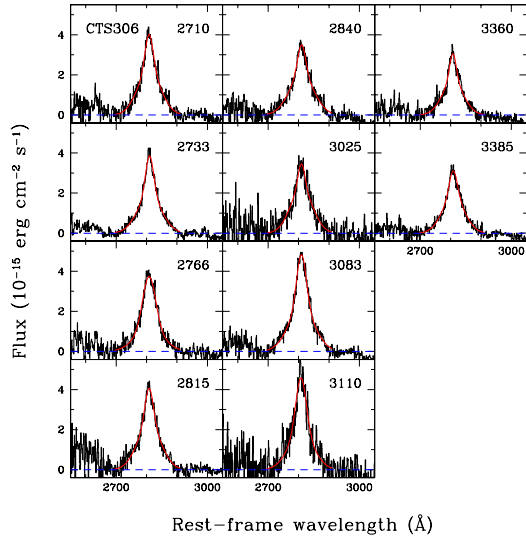


FIG. 3.— As in Figure 2 for CTS306.

The random error on the MgII line flux measurements is typically 3% level (Table 3). By adding $\sim 2\%$ systematic error of the flux calibration to the random error, we take 5% as an upper limit to the total error of the MgII line flux measurements. A series of continuum-subtracted spectra for individual objects are presented in Figures 2-6, where variation of the MgII line flux can be qualitatively detected.

From each spectrum the monochromatic continuum flux was measured at 3000\AA by averaging the flux within 40\AA window. We note that the size of the window does not affect the continuum variability. Typical errors on the continuum flux measurements were 2%-3% depending on the S/N of each spectrum (see Table 3).

3.4. Flux variability of the MgII line and continuum

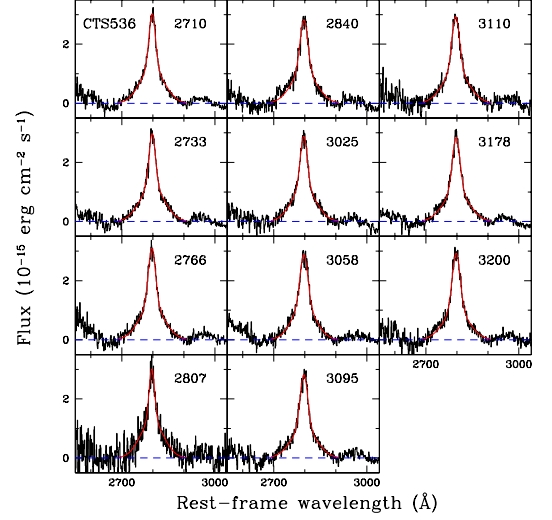


FIG. 4.— As in Figure 2 for CTS536.

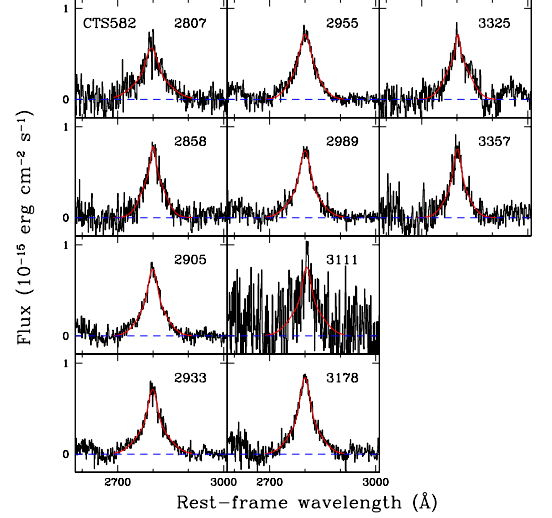


FIG. 5.— As in Figure 2 for CTS582.

In Figure 7 we present light curves of the MgII line flux (left) and the continuum flux at 3000\AA (right). All five quasars showed continuum (3000\AA) flux variability, with peak-to-peak variations of 17%-38% and rms variations of 6%-15%. Continuum flux variation shows consistent pattern as B band flux variation in the case of CTS536, for which the MgII line flux has been almost constant during the monitoring period. However, for the other objects, the continuum flux variations are different from B band flux variations depending on the relative contribution of the MgII line flux.

In the case of MgII line flux, we detected 23%-50% peak-to-peak changes and 8%-17% rms variations for four objects. In contrast, one object, CTS536, did not show clear variation within the measurement error 5%. The MgII line flux variation of these four quasars is similar to that of local Seyfert galaxies and high redshift quasars (e.g. Clavel et al. 1991; Trevese et al. 2007),

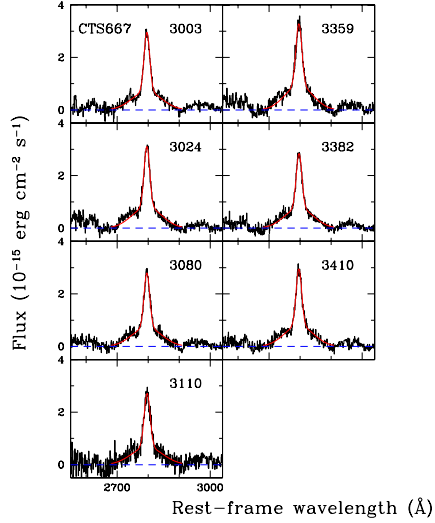


FIG. 6.— As in Figure 2 for CTS667.

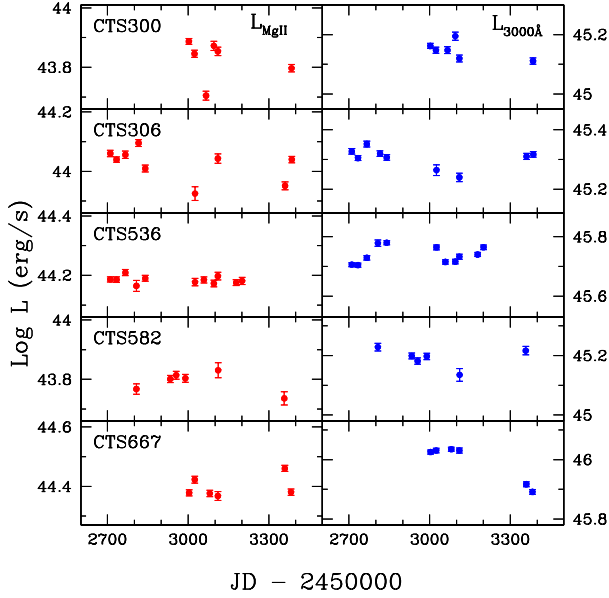


FIG. 7.— Variability of the MgII line flux (left panels) and the continuum flux at 3000 Å (right panels) for the sample.

implying that intermediate redshift quasars have similar characteristics of the MgII line flux variability, although the actual amplitude is highly variable depending on individual objects and the monitoring time base-line.

3.5. Line width variability

To measure the MgII line width, we fit the line profile with multi-Gaussian models and determine the best fit model based on χ^2 statistics. Fitting the line profile is necessary for low quality spectra, for which FWHM can not be easily defined on the data. We measured FWHM on the best fit model as demonstrated in Figures 2-6 (red lines). In the case of CTS667, FeII contamination is present in the wings of the MgII line profile and our multi-Gaussian model also fits the broad FeII component. However, FWHM of the MgII line is not significantly af-

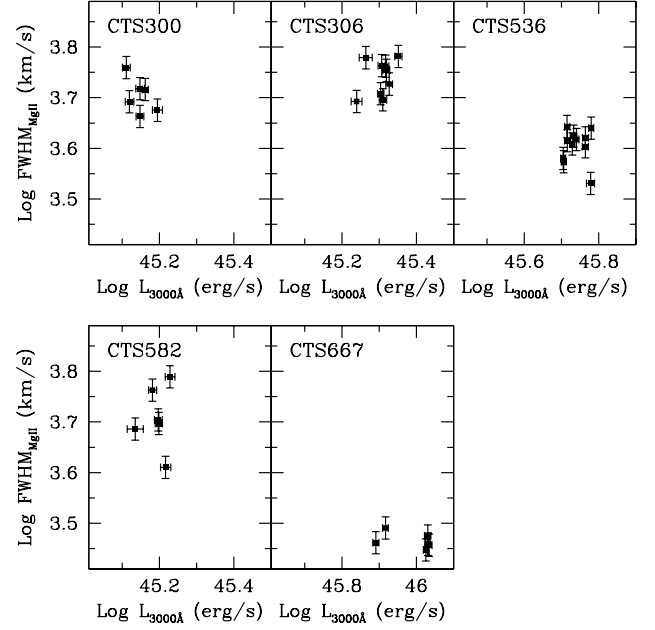


FIG. 8.— MgII line width variability. 5% error was assumed for the FWHM measurements.

ected by the shape of the wings. Thus, we simply ignored the FeII component although this will increase the uncertainties of MgII line width measurements, which is dominated by systematic errors from continuum subtraction and assumed to be $\sim 5\%$.

In Figure 8 we compared measured FWHM with the continuum luminosity for each object. The rms variation of the MgII line width, ranging from 4% to 15% (see Table 3), is similar to the rms variation of continuum flux, suggesting a photoionization origin of the MgII line. The reason why we do not clearly see a correlation between the line width and continuum luminosity, as expected from a photoionization model (e.g. $\text{FWHM} \propto L_{3000\text{\AA}}^{1/2}$), is probably due to the combined effects of measurement and systematic errors on the line width and relatively small flux variations of the continuum.

3.6. Black hole mass estimates

We estimated black hole mass using the virial technique based on the empirical size-luminosity relation of the reverberation sample (Kaspi et al. 2005; Bentz et al. 2006). Combining the MgII line FWHM and the continuum luminosity at 3000 Å, measured from the mean spectra of each object, black hole mass was determined with the empirical formula from McGill et al. (2007):

$$M_{BH} = 6.77 \left(\frac{L_{3000}}{10^{44} \text{ erg s}^{-1}} \right)^{0.47} \left(\frac{\text{FWHM}_{\text{MgII}}}{1000 \text{ km s}^{-1}} \right)^2 M_{\odot}. \quad (1)$$

The estimated black hole mass of the sample quasars ranges between $10^{8.6}$ and $10^{8.9} M_{\odot}$ (see Table 1). By multiplying a factor of 5.9 to the continuum luminosity at 3000 Å (McLure & Dunlop 2004), we estimated bolometric luminosity and computed the Eddington ratio. The determined Eddington ratio ranges from 0.1 to

TABLE 3
VARIABILITY MEASUREMENTS

Target (1)	N (2)	N (3)	MgII (4)	rms (5)	error (6)	L ₃₀₀₀ (7)	rms (8)	error (9)	F (10)	rms (11)	F (12)	L ₃₀₀₀ (13)
CTS300	8	6	.17 (50%)	.067 (17%)	.013 (3%)	.08 (20%)	.028 (7%)	.011 (3%)	5051	.035 (8%)	5197	45.15
CTS306	10	9	.16 (45%)	.054 (13%)	.013 (3%)	.12 (32%)	.032 (8%)	.011 (3%)	5494	.035 (8%)	5540	45.30
CTS536	11	11	.04 (10%)	.012 (3%)	.011 (3%)	.07 (17%)	.027 (6%)	.008 (2%)	4020	.033 (8%)	4101	45.74
CTS582	10	6	.13 (35%)	.034 (8%)	.017 (4%)	.09 (23%)	.030 (7%)	.013 (3%)	5102	.063 (15%)	5144	45.19
CTS667	7	6	.09 (23%)	.036 (9%)	.012 (3%)	.14 (38%)	.060 (15%)	.008 (2%)	2907	.015 (4%)	2862	45.99

NOTE. — Col. (1): Target ID. Col. (2): Number of observed epochs for spectroscopy. Col. (3): Number of epochs with flux calibration using available photometry. Col. (4): peak to peak variation of MgII line flux in logarithmic scale. Col. (5): rms variation of MgII line flux in logarithmic scale. Col. (6): mean error on MgII line flux measurement in logarithmic scale. Col. (7): peak to peak variation of continuum luminosity at 3000Å in logarithmic scale. Col. (8): rms variation of continuum luminosity at 3000Å in logarithmic scale. Col. (9): mean error on continuum luminosity measurement in logarithmic scale. Col. (10): mean FWHM of the MgII line in km s⁻¹. Col. (11): rms variation of FWHM in logarithmic scale. Col. (12): FWHM of the MgII line in km s⁻¹, measured from mean spectra. Col. (13): L_{3000Å} in erg s⁻¹, measured from mean spectra.

1.1 as tabulated in Table 1, indicating our sample quasars are highly accreting luminous quasars.

4. DISCUSSION AND CONCLUSIONS

We monitored and measured variability of 5 high-luminosity quasars at $0.4 \lesssim z \lesssim 0.6$. From the photometry, we detected 10%-24% peak-to-peak flux variations and 3%-8% rms variations in the B band which corresponds to the rest-frame 2500Å-3600Å range. After spectroscopic flux calibration using photometric measurements, we measured the MgII line flux and the continuum flux at 3000Å from the observed spectra. MgII flux variations were detected for 4 objects with 23%-50% peak-to-peak variations and 8%-17% rms variations. One object did not show clear variations in the MgII line flux within the measurement error (~5%) over the two year monitoring period. By measuring FWHM of the MgII line, we measured variability of line width for the same quasars, which showed 4%-15% rms variations.

These variability detections are consistent with a picture that the MgII line is variable as other broad lines, such as Balmer lines or high ionization lines (Ly α and CIV). The MgII line of these intermediate redshift quasars probably originates in the same region as H β , as shown in the cases of NGC 3783 and NGC 4151, for which similar time-lags were measured from H β and MgII lines (Reichert et al. 1994; Peterson et al. 2004; Metzroth et al. 2006). It is possible that for some particular objects MgII line emitting region is more extended than H β line emitting region, and hence MgII line variability may not be detected in short time scales. This scenario was suggested for NGC 3516, which showed no MgII line flux variations (Goad et al. 1999). However, it is not clear whether NGC 3516 is an abnormal object with an extended MgII line region, or substantial fraction of quasars have a similarly extended MgII line region. Monitoring flux variations of the MgII line together with the H β line

using a larger sample of AGNs is necessary to properly address these issues.

Although we did not attempt to do reverberation analysis due to the short time baseline with insufficient numbers of epochs, it is shown that the MgII line can be used for reverberation mapping for even luminous quasars at intermediate redshifts. Compared to the local Seyfert galaxies, a longer-term monitoring program is necessary for these objects due to the 1+z effect on the observed time scale as well as larger intrinsic reverberation time scales for more luminous quasars. The estimated time-lags for the sample quasars, based on the continuum luminosity at 3000Å and the size-luminosity relation (McLure & Dunlop 2004), range from 74 to 217 light-days. Thus, a few year monitoring program with synchronous photometry and spectroscopy can reveal the reverberation time scales of the MgII line for the sample. Small telescopes (1-3m) can be very useful tools for MgII line reverberation mapping since MgII is much stronger than H β which has been generally used in reverberation mapping of local AGNs. Regular monitoring and service observation is a key for a success in future reverberation mass measurements.

This work is based on data collected at the CTIO through the SMARTS consortium. I am grateful to Meg Urry for support and the inspiration for the project during my stay at the Yale Center for Astronomy and Astrophysics. I thank Tommaso Treu and Charles Bailyn for useful discussions and suggestions and the referee for useful suggestions. I thank all CTIO staffs for service observations, Rebecca Winnick for scheduling, and Brendan Cohen for data collection and initial reduction works. I specially thank Suzanne Tourtellotte for data archiving and handling.

REFERENCES

- Bentz, M. C., Peterson, B. M., Pogge, R. W., Vestergaard, M., & Onken, C. A. 2006, *ApJ*, 644, 133
 Bonning, E. W., Cheng, L., Shields, G. A., Salvander, S., & Gebhardt, K. 2007, *ApJ*, 659, 211
 Blandford, R. D., & McKee, C. F. 1982, *ApJ*, 255, 419
 Clavel, J., et al. 1991, *ApJ*, 366, 64
 Croton, D. J., et al. 2006, *MNRAS*, 365, 11
 Di Matteo, T., Springel, V., & Hernquist, L. 2005, *Nature*, 433, 604
 Davis, S. W., Woo, J.-H., & Blaes, O. M. 2007, *ApJ*, in press (astro/07071456)
 Goad, M. R., Koratkar, A. P., Kim-Quirano, J., Korista, K. T., O'Brien, P. T., & Axon, D. J. 1999, *ApJ*, 524, 707

- Kaspi, S., Smith, P. S., Netzer, H., Maoz, D., Jannuzi, B. T., & Givon, U. 2000, *ApJ*, 533, 631
- Kaspi, S., Maoz, D., Netzer, H., Peterson, B. M., Vestergaard, M., & Jannuzi, B. T. 2005, *ApJ*, 629, 61
- Kaspi, S., Brandt, W. N., Maoz, D., Netzer, H., Schneider, D. P., & Shemmer, O. 2007, *ApJ*, 659, 997
- Maza, J., Ruiz, M. T., Gonzalez, L. E., Wischnjewsky, M., & Antezana, R. 1993, *Revista Mexicana de Astronomia y Astrofisica*, 25, 51
- Maza, J., Ortiz, P. F., Wischnjewsky, M., Antezana, R., & Gonzalez, L. E. 1995, *Revista Mexicana de Astronomia y Astrofisica*, 31, 159
- Maza, J., Wischnjewsky, M., & Antezana, R. 1996, *Revista Mexicana de Astronomia y Astrofisica*, 32, 35
- McGill, K. L., Woo, J.-H., Treu, T., & Malkan, M. A. 2007, *ApJ*, 673, 703
- McLure, R. J., & Dunlop, J. S. 2004, *MNRAS*, 352, 1390
- Metzroth, K. G., Onken, C. A., & Peterson, B. M. 2006, *ApJ*, 647, 901
- Netzer, H. & Trakhtenbrot, B. 2007, *ApJ*, 654, 754
- Peterson, B. M., Wanders, I., Bertram, R., Hunley, J. F., Pogge, R. W., & Wagner, R. M. 1998, *ApJ*, 501, 82
- Peterson, B. M., et al. 2004, *ApJ*, 613, 682
- Reichert, G. A., et al. 1994, *ApJ*, 425, 582
- Trevese, D., Paris, D., Stirpe, G. M., Vagnetti, F., & Zitelli, V. 2007, *A&A*, 470, 491
- Treu, T., Woo, J.-H., Malkan, M. A., & Blandford, R. D. 2007, *ApJ*, 667, 117
- Vestergaard, M. 2002, *ApJ*, 571, 733
- Vestergaard, M. 2004, *ApJ*, 601, 676
- Wandel, A., Peterson, B. M., & Malkan, M. A. 1999, *ApJ*, 526, 579
- Webb, & Malkan, A. 2000, *ApJ*, 540, 652 *ApJ*, 601, 676
- Woo, J.-H., & Urry, C. M. 2002, *ApJ*, 579, 530
- Woo, J.-H., Treu, T., Malkan, M. A., & Blandford, R. D. 2006, *ApJ*, 645, 900
- Woo, J.-H., Treu, T., Malkan, M. A., Ferry, M. A., & Misch, T. 2007, *ApJ*, 661, 60